High energy octupole resonance in ^{116}Sn

H. L. Clark, D. H. Youngblood, and Y.-W. Lui
Cyclotron Institute, Texas A&M University, College Station, Texas 77843
(Received 10 August 1995)

The region of excitation energy from $7 \leqslant E_x \leqslant 38$ MeV in ^{116}Sn was studied with inelastic scattering of 240 MeV α particles. Parameters obtained for the isoscalar giant monopole resonance and the isoscalar giant quadrupole resonance are in agreement with accepted values. A peak exhausting $(67 \pm 10)\%$ of the $E3$ energy-weighted sum rule at $E_x = 21.8 \pm 0.5$ MeV with width $\Gamma = 7.1 \pm 0.5$ MeV was identified as the isoscalar high energy octupole resonance (HEOR). The energy and width are consistent with previous measurements made with proton, ^{3}He, and α particle projectiles. The observed strength of the HEOR is in agreement with measurements made with ^{3}He inelastic scattering, but is roughly three to four times larger than measurements made with α particle and proton inelastic scattering. [S0556-2813(96)01407-0]

PACS number(s): 24.30.Cz, 21.60.Ev, 25.55.Ci, 27.60.+j

I. INTRODUCTION

The high energy octupole resonance (HEOR) has been studied in a wide range of nuclei ranging from $40 \leqslant A \leqslant 238$ with a variety of projectiles including electrons [1–5], protons [6,7], ^{3}He [8], α particles [9,10], and heavy ions [11,12]. The tin isotopes ^{116,118,120}Sn have been investigated extensively and the energy-weighted sum rule (EWSR) strengths, widths (Γ), and excitation energies (E_x) obtained are shown in Figs. 1(a), 1(b), and 1(c), respectively. Figures 1(b) and 1(c) show that in the tin isotopes the excitation energy and width are consistently around 23 and 7 MeV, respectively. Figure 1(a) shows that the measured $E3$ strengths vary tremendously, and those obtained for ^{116}Sn from inelastic α scattering ($\leqslant$19% of the $E3$ EWSR) are well below the expected values. Measurements made with 129 MeV inelastic α scattering on ^{116}Sn identified $(31 \pm 6)\%$ of the $E3$ EWSR in a low lying $J^\pi = 3^-$ state and the low energy octupole resonance (LEOR) [13]. The remainder of the $E3$ strength ($\sim$70%) should reside in the HEOR.

Inelastic scattering of α particles at energies between 90 and 172 MeV has been very effective for investigating isoscalar giant resonances ($T=0$), in part because isovector giant resonances ($T=1$) are weakly excited. However, this beam energy range is not suitable for investigating the HEOR in ^{116}Sn. At these energies, α particles from the pickup-breakup reactions $(\alpha, ^5\mathrm{He}) \rightarrow (\alpha, \alpha n)$ and $(\alpha, ^5\mathrm{Li}) \rightarrow (\alpha, \alpha p)$ show up as broad bumps in the continuum over the excitation region of the HEOR. At $E_\alpha = 96$ MeV, α particles from these processes have energies between 59 and 79 MeV [14], and thus appear the same in α particle spectra as inelastic scattering peaks from states with excitation energies between 17 and 37 MeV, which clearly overlap the HEOR. As the bombarding energy is increased, the apparent excitation energy of the pickup-breakup peaks increases (this is the method used to distinguish them from inelastic excitations). However, even at 172 MeV, the pickup-breakup peaks begin at $E_x = 26$ MeV, which overlaps the tail of the HEOR and may complicate the assessment of the continuum. α particle studies of the HEOR in ^{116}Sn have been carried out at $E_\alpha = 340$ and 480 MeV [10], where the pickup-breakup peaks appear above an equivalent excitation energy of 50 MeV and are not a factor. However, in these studies, very low EWSR strengths were obtained for even the well-known isoscalar giant quadrupole (GQR) and isoscalar giant monopole (GMR) resonances in ^{116}Sn. Furthermore, isovector strength is more strongly excited at these energies [15], and the isovector quadrupole resonance at $E_x \sim 27$ MeV [16] may make observation of the HEOR more difficult. We have therefore investigated the isoscalar HEOR in ^{116}Sn with 240 MeV α particles. At this energy, the products from ^{5}He-^{5}Li pickup-breakup reactions are well past the region of interest ($E_x \geqslant 35$ MeV) and the contribution from isovector resonances should be negligible.

II. EXPERIMENTAL TECHNIQUE

Beams of 240 MeV α particles from the Texas A&M K500 superconducting cyclotron bombarded a self-supporting foil enriched to 95.74% in ^{116}Sn in the target chamber of the multipole-dipole-multipole (MDM) spectrometer [17]. The target thickness, determined by weighing, was 5.74 ± 0.57 mg/cm^2. Scattered particles which passed the spectrometer acceptance were analyzed by the MDM spectrometer and were detected by the modified Oxford detector. Details of the detector and spectrometer were reported in Refs. [18–21] and [22], respectively.

Data on both elastic and inelastic scattering were taken at two separate times which utilized slightly different experimental setups. In the first run (set 1), data were acquired over the angle range $4° \leqslant \theta \leqslant 8°$ using a solid-angle-defining collimator with $\Delta\theta = 4°$ and $\Delta\phi = 2°$. In the second run (set 2), data were acquired over the angle range $2° \leqslant \theta \leqslant 6°$ using a solid-angle-defining collimator with $\Delta\theta = 4°$ and $\Delta\phi = 4°$. The newly installed beam analysis system (BAS) [23] was also utilized for data acquired in set 2, which helped to reduce beam halo and improve beam momentum resolution. For the giant resonance data, elastically scattered α particles were stopped at the detector entrance.

Ray tracing was used to determine the horizontal component of the scattering angle θ; however, ϕ was not measured, so the effects of the different vertical openings were accounted for by angle averaging and will be discussed later. An angular resolution of $\Delta\theta = 0.15°$ was obtained by placing

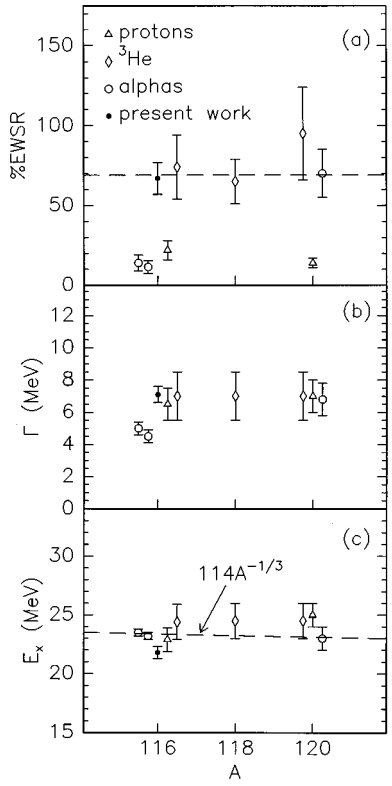

FIG. 1. Comparisons of HEOR data for the tin isotopes from this work (closed circles) and others (triangles [6,7], diamonds [8], and open circles [9,10]). (a) The %EWSR strength as a function of A. The dashed line represents the $E3$ EWSR strength remaining after the subtraction of strength in the low lying 3^- state and the LEOR in ^{116}Sn as reported by Ref. [13]. (b) The width as a function of A. (c) E_x as a function of A. The dashed line represents a prediction using the harmonic-oscillator shell model approximation [35].

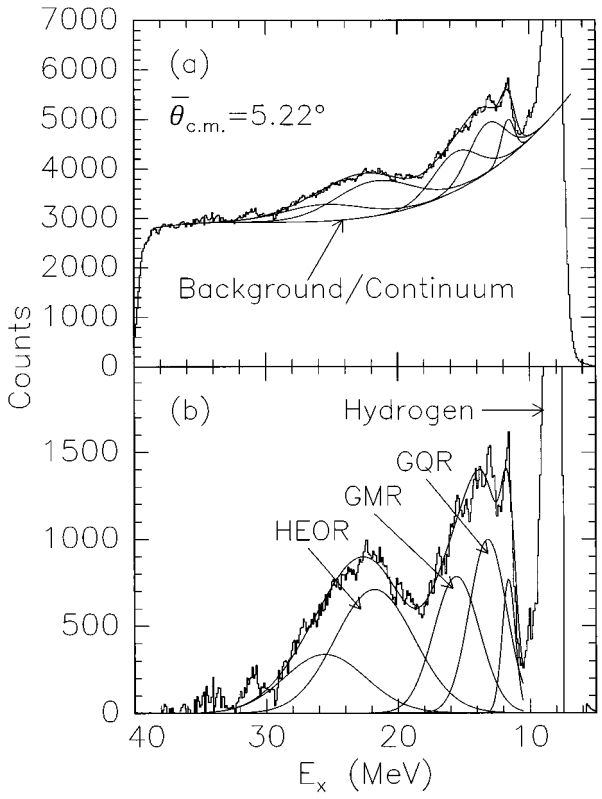

FIG. 2. α particle spectrum taken at $\overline{\theta}_{c.m.}=5.22°$ plotted versus excitation energy for ^{116}Sn(α,α'). (a) The raw spectrum with lines showing the result of a five-peak multispectrum fit and background/continuum. (b) The spectrum with background/continuum subtracted and the result of a five-peak multispectrum fit. The GMR, GOR, and HEOR are indicated.

a software window on angle deviation as described in Ref. [20]. The spectrometer angle was verified from the kinematic crossover of elastic scattering from hydrogen with ^{12}C excited states. For a given spectrometer field setting, the focal plane position was calibrated in α particle momentum from the locations of peaks from ^{12}C excited states (7.65 to 24.0 MeV [24]).

III. DATA ANALYSIS

Each data set was divided into ten subsets of data (20 spectra in all), each corresponding to $\Delta\theta\approx0.4°$ using the angle obtained from ray tracing. A giant resonance spectrum taken at the average center-of-mass angle $\theta_{c.m.}=5.22°$ is shown in Fig. 2(a). The average angle (θ) was obtained by integrating over the angle bin width and height (determined by the vertical dimension of the collimator). Absolute cross sections were determined by normalizing the elastic scattering data to optical-model calculations. Cross sections for the giant resonance data were obtained by normalizing the giant resonance spectra to the elastic spectra in the region of excitation energy between 10 and 20 MeV.

Optical-model calculations were performed with the code PTOLEMY [21,25] using ^{116}Sn parameters [21] (listed in Table I) we obtained in a previous study. Angle-weighted-average cross sections were obtained for the different vertical dimensions of the collimators. Figure 3 shows the elastic scattering data and the optical-model calculations plotted versus average angle. The error bars include statistical error and angle uncertainty (summed in quadrature). The angular distributions obtained with different vertical dimensions of the collimators differ significantly only for $\theta_{c.m.}\leqslant2.5°$.

The giant resonance data were analyzed by first subtracting a background/continuum and then performing a multiple peak fit. For each spectrum, several assumptions for the background/continuum were made to test the effects of different backgrounds. They were generally drawn [as indicated in Fig. 2(a)] from high to low excitation energy as a smooth curve (fourth-order polynomial) that was extrapolated from the slope of the continuum at high excitation energy (beyond $\sim$30 MeV) and then curved up to the minimum in the spectrum on the low excitation side. For the HEOR region ($E_x\geqslant20$ MeV), the curves obtained with the different assumptions were nearly the same. They differed only in the

TABLE I. Optical-model parameters [21] for ^{116}Sn at $E_\alpha=240$ MeV.

V (MeV)	W (MeV)	R_v (fm)	R_w (fm)	a_v (fm)	a_w (fm)	R_c (fm)
88.0	21.4	5.89	7.05	0.83	0.80	6.34

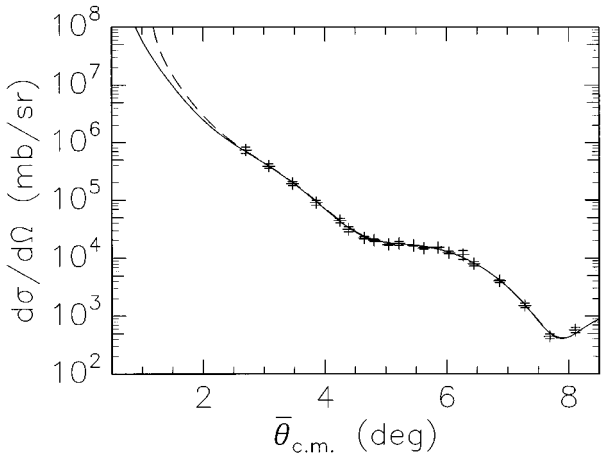

FIG. 3. The elastic scattering differential cross section obtained for 240 MeV α scattering on ^{116}Sn is plotted versus average center-of-mass angle. The solid line and dashed line represent angle-weighted-average optical-model calculations for $\Delta\phi=2°$ and 4°, respectively.

region $E_x \leq 20$ MeV. The effects of the different background/continuum show mainly in the EWSR strengths and will be discussed later.

Spectra which did not contain the peak due to elastic scattering off hydrogen were fitted simultaneously with a multipeak-multispectra fitting routine with the requirement that all peaks have the same excitation energy and width in each spectrum [26]. Excellent fits to the spectra could be obtained with three peaks in addition to the well-known GMR and GQR. Figures 2(a) and 2(b) illustrate a spectrum taken at $\theta_{c.m.}=5.22°$ with and without background/continuum subtracted, and the results of the five-peak multispectra fit. The positions and widths from Ref. [27] were used as initial parameters for the GMR and GQR. The best multipeak-multispectra fit ($\chi^2\sim 2$) was obtained for positions and widths of the GQR and GMR fixed at $E_x=13.2$ MeV and $\Gamma=3.3$ MeV for the GQR and $E_x=15.6$ MeV and $\Gamma=4.1$ MeV for the GMR [27]. The heights of the GQR and GMR as well as all parameters of the other three peaks were allowed to vary. The positions and widths obtained for the other peaks are given in Table II. For the spectra where elastic scattering off hydrogen in the target obscured the GMR and GQR peaks ($\theta_{c.m.} \geq 6.45°$), three-peak single-spectra fits were performed to the excitation region $10 \leq E_x \leq 30$ MeV. In these spectra, the positions and widths of the $E_x=21.8$ and 26.1 MeV peaks were fixed at the values obtained from the five-peak multispectra fit. The heights of these peaks and the parameters of the peak due to elastic scattering off hydrogen were free to vary. Spectra taken at $\theta_{c.m.}=3.08°$, 3.47°, and 3.86° were excluded from the analysis because, at the spectrometer field setting used, elastically scattered α particles were deflected off the spectrometer exit and into the detector, which created a broad bump in the region of interest. This bump was well below the region of interest for the $\theta_{c.m.}=2.70°$ spectra and well above the region of interest for spectra with $\theta_{c.m.} \geq 4.25°$.

A four-peak multispectrum fit was also attempted. The GMR and GQR positions and widths were fixed at the values stated above. The rest of the parameters were allowed to vary, and the best fit was obtained with a narrow peak at 11.4 MeV and a broad peak ($\Gamma=11.2$ MeV) at $E_x=23.0$ MeV. The quality of the fit ($\chi^2\sim 10$) was much worse than the five-peak fit because the broad peak had different shapes in the different spectra.

The angular distributions obtained for the peaks are shown in Fig. 4. The angular distribution of the narrow peak at $E_x=11.4$ MeV was inconsistent and is not shown. Distorted-wave Born approximation (DWBA) calculations are also shown, and with the exception of the peak at $E_x=26.1$ MeV, agree very well with the data. The error bars on the data points represent the combined uncertainty (summed in quadrature) due to statistics and the quality of the multipeak fit. The cross sections for the background/continuum in the region $15 \leq E_x \leq 30$ MeV from both data sets are also shown in Fig. 4, and the error bars are due statistical uncertainties only. The reduction in the cross section for the background/continuum in set 2 (closed circles) is due to the use of the BAS (which reduced beam halo) and the larger vertical dimension of the collimator (allowing $\Delta\phi=4°$, which reduced elastic slit scattering). The vertical dimension of the collimator was smaller (allowing $\Delta\phi=2°$)

TABLE II. Five-peak multispectra fit parameters and EWSR values from this work and results from other work on ^{116}Sn. An asterisk implies the values were fixed in the fits.

Work	Projectile, E (MeV)	J^π	E_x (MeV)	Γ (MeV)	%EWSR
Present	α, 240	3^-	21.8±0.5	7.1±0.5	67±10
Ref. [10]	α, 340		23.5±0.3	5.0±0.4	14±5
Ref. [10]	α, 480		23.2±0.3	4.5±0.3	11.5±4
Ref. [8]	^{3}He, 110–140		24.4±1.5	7.0±1.5	74±20
Ref. [6]	p, 800		22.9±1.0	6.5±1.0	22±6
Present	α, 240	0^+	15.6*	4.1*	100±15
Ref. [27]	α, 129		15.6±0.3	4.1±0.3	180±60
Present	α, 240	2^+	13.2*	3.3*	95±20
Ref. [27]	α, 129		13.2±0.2	3.3±0.2	84±24
Present	α, 240		26.1±0.6	7.3±0.4	
Present	α, 240		11.4±0.4	0.4±0.1	

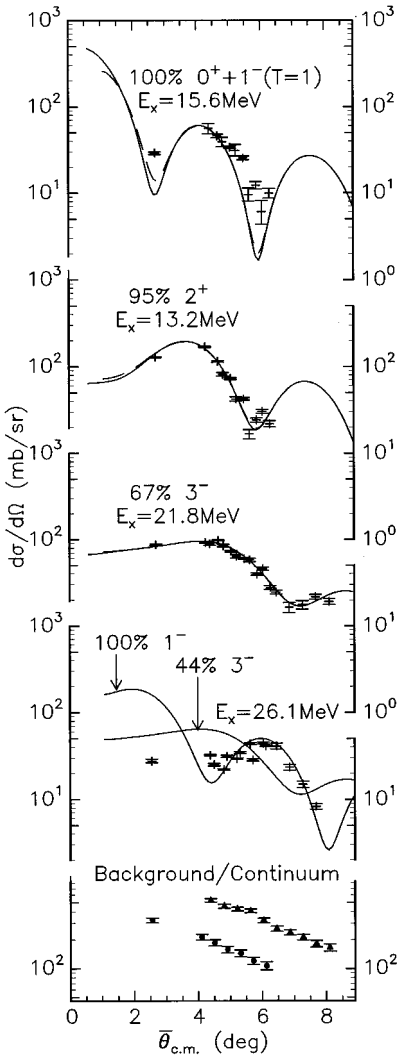

FIG. 4. Angular distributions of the differential cross sections of the peaks and the underlying background/continuum plotted versus the average center-of-mass angle. The curves represent DWBA calculations for the indicated resonances where the solid lines and dashed lines have been angle averaged for $\Delta\phi=2°$ and 4°, respectively. The solid triangles and circles represent the background/continuum from set 1 and set 2, respectively.

and the BAS was not available for the data acquired in set 1 (closed triangles).

For each state, the EWSR strengths were calculated by normalizing the differential cross sections to the DWBA calculations. The normalization is quoted as the square of the deformation parameter (β^2), and the fraction of the EWSR strength exhausted by the resonance is determined by the ratio of the square of the experimental and theoretical deformation lengths (β^2R^2, where R is the nuclear radius). The errors in the EWSR strengths were determined by the amount that the DWBA calculations could deviate from the best fit and still cross through the *combined* uncertainty. The combined uncertainty was determined from statistics, fit quality, and fluctuations in the cross section due to different assumptions for the background/continuum (all summed in quadrature). The results with errors are listed in Table II.

The GQR and HEOR DWBA calculations were performed with the code PTOLEMY with internal collective form factors [$U(r)$] of the usual form,

$$U(r)=R\,\frac{dU_0(r)}{dr}, \tag{3.1}$$

where R is the optical-model nuclear radius and $U_0=V+iW$ is the optical-model potential with real (V) and imaginary (W) potentials of the Woods-Saxon form. For such states located at excitation energy E_x that exhaust 100% of the EWSR strength, the theoretical deformation length is

$$\beta_L^2R^2=L(2L+1)\,\frac{\hbar^2}{2mE_x}\,\frac{4\pi}{3A}, \tag{3.2}$$

where β_L is the deformation parameter and L is the angular momentum of the state. Recently, Beene, Horen, and Satchler [28] showed that the deformed optical potential model does not correctly predict $E3$ strength for low lying states excited by ^{17}O inelastic scattering; however, the value we obtained [21] [using Eqs. (3.1) and (3.2)] for the $E3$ deformation length of the 2.266 MeV state in ^{116}Sn measured with 240 MeV inelastic α scattering agrees with values obtained from inelastic electron scattering [29,30].

The isovector giant dipole resonance (IVGDR) calculation was also performed with PTOLEMY by reading in an external form factor. The form factor and EWSR for the IVGDR are described in Ref. [31]. For convenience, the GMR and isoscalar giant dipole resonance (ISGDR) calculations were performed with the code DWUCK4 [32] using internal form factors. A comparison of calculations with DWUCK4 and PTOLEMY for 240 MeV α particles is described in Ref. [21]. The GMR and ISGDR form factors are expressed as

$$U(r)=-3U_0(r)-r\,\frac{dU_0(r)}{dr}\quad\text{for } L=0,$$

$$U(r)=\frac{1}{R\sqrt{3}}\left(-3r^2\,\frac{dU_0(r)}{dr}-10rU_0(r)+\frac{5}{3}\langle r^2\rangle_{\rm WS}\,\frac{dU_0(r)}{dr}\right)\quad\text{for } L=1, \tag{3.4}$$

from Refs. [33] and [34], respectively, where $\langle r^2\rangle_{\rm WS}$ is the mean squared radius of the Woods-Saxon optical-model potential. For the GMR and ISGDR which exhaust the EWSR limit, the theoretical deformation lengths are expressed as

$$\beta_0^2R^2=\frac{\hbar^2}{2mE_x}\,\frac{20\pi}{3A}\quad\text{for } L=0, \tag{3.5}$$

$$\beta_1^2R_{1/2}^2=\frac{6\pi\hbar^2R_{1/2}^4}{mAE_x}\,(11\langle r^4\rangle_{\rm FM}-\tfrac{25}{3}\langle r^2\rangle_{\rm FM}^2)^{-1}$$

$$\text{for } L=1, \tag{3.6}$$

from Refs. [33] and [34], respectively, where $R_{1/2}$ and $\langle r^n\rangle_{\rm FM}$ are the half-density radius and mean radius to the nth power of the Fermi mass distribution. For both the Woods-Saxon

and Fermi mass distributions, the values for $\langle r^n \rangle$ were obtained by numerical integration.

IV. DISCUSSION

We obtained consistent fits to the spectra over the excitation energy range $11 \leq E_x \leq 30$ MeV with five peaks, of which three could be identified as the GMR, GQR, and HEOR. The strengths obtained for the GMR and GQR were $(100 \pm 15)\%$ of the $E0$ EWSR and $(95 \pm 20)\%$ of the $E2$ EWSR, respectively, and are consistent with the results for ^{116}Sn from Refs. [10] and [27]. The strength obtained for the HEOR was $(67 \pm 10)\%$ of the $E3$ EWSR. In other ^{116}Sn work, $(31 \pm 6)\%$ of the $E3$ EWSR has been identified in the sum of the low lying $J^{\pi}=3^{-}$ state and the LEOR [13]. Therefore the strength of these states plus our strength for the HEOR then exhaust roughly 100% of the $E3$ EWSR. The width ($\Gamma=7.1$ MeV) of the HEOR is also in good agreement with previous measurements on the tin isotopes performed with protons [6,7], ^{3}He [8], and α particles [9].

Bonin *et al.* [10] report much lower strength for the HEOR [$(14 \pm 5)\%$ and $(11.5 \pm 4)\%$] in ^{116}Sn from 340 and 480 MeV inelastic α scattering, but they also only see 43% and 49% of the $E2$ EWSR in the GQR and 28% and 22% of the $E0$ EWSR in the GMR, where $\sim$100% of each are observed in our measurement and are reported in numerous other experiments. Carey *et al.* [6] report 22% of the $E3$ EWSR in the HEOR in ^{116}Sn using 800 MeV inelastic proton scattering, but do not report the strengths they obtained for the other resonances they observed. This is particularly important, since the GMR overlaps the HEOR, and the two resonances can only be separated by a multiple peak fitting routine. However, Bertrand *et al.* [7], also using inelastic proton scattering, report similar low values of the $E3$ EWSR for the HEOR in ^{120}Sn but also see only $\sim$35% of the $E2$ EWSR in the GQR.

The position we obtained for the HEOR ($E_x=21.8$ MeV) is slightly lower than previous measurements ($E_x \sim 23.5$ MeV); however, the peak at $E_x=26.1$ MeV has not been previously reported in ^{116}Sn. If the excitation region containing these two peaks is fitted by one peak, the position and width are $E_x=23.0$ MeV and $\Gamma=11.2$ MeV, respectively. This position is consistent with the previous average for the HEOR, but the width is much too large. Furthermore, as the angular distributions for the 21.7 and 26.1 MeV states differ, the χ^2 for the fit of the broad peak becomes considerably worse. As shown in Fig. 4, the ISGDR DWBA calculation fits the angular distribution for the 26.1 MeV peak above $\theta_{\text{c.m.}}=4°$, but the $\theta_{\text{c.m.}}=2.70°$ data point is much too low. From the present data we cannot clearly identify the 26.1 MeV peak as the ISGDR due to this discrepancy, and also since the cross section for this peak at large angles has large errors, as it is near the detector cutoff. A future measurement in ^{116}Sn and other nuclei, in this excitation region and over the angles $1° \leq \theta_{\text{sp}} \leq 8°$, is presently being planned. If the peak is indeed the ISGDR it should be much stronger than the HEOR at small angles $\theta_{\text{c.m.}} \leq 3°$.

ACKNOWLEDGMENTS

We thank Patrick Oliver and George Simler for their assistance in taking the data. This work was supported in part by the U.S. Department of Energy under Grant No. DE-FE05-86ER40256 and by the Robert A. Welch Foundation.

[1] S. Fukada and Y. Torizuka, Phys. Lett. **62B**, 146 (1976).
[2] K. Hosoyama and Y. Torizuka, Phys. Rev. Lett. **35**, 199 (1975).
[3] M. Sasao and Y. Torizuka, Phys. Rev. Lett. **30**, 1068 (1973); Phys. Rev. C **15**, 217 (1977).
[4] R. Pitthan, F. R. Buskirk, E. B. Dally, J. N. Dyer, and X. K. Maruyama, Phys. Rev. Lett. **33**, 849 (1974); **34**, 848 (1975).
[5] M. Nagao and Y. Torizuka, Phys. Rev. Lett. **30**, 1068 (1972).
[6] T. A. Carey, W. D. Cornelius, N. J. DiGiacomo, J. M. Moss, G. S. Adams, J. B. McClelland, G. Pauletta, C. Whitten, M. Gazzaly, N. Hintz, and C. Glashausser, Phys. Rev. Lett. **45**, 239 (1980).
[7] F. Bertrand, E. E. Gross, D. J. Horen, J. R. Wu, J. Tinsley, D. K. McDaniels, L. W. Swenson, and R. Liljestrand, Phys. Lett. **103B**, 326 (1981).
[8] T. Yamagata, S. Kishimoto, K. Yusa, K. Iwamoto, B. Saeki, M. Tanaka, T. Fukuda, I. Miura, M. Inoue, and H. Ogata, Phys. Rev. C **23**, 937 (1981).
[9] H. P. Morsch, M. Rogge, P. Turek, P. Decowski, L. Zemlo, C. Mayer-Böricke, S. A. Martin, G. P. A. Berg, I. Katayama, J. Meissburger, J. G. M. Römer, J. Reich, P. Wucherer, and W. Bräutigam, Phys. Lett. **119B**, 311 (1982).
[10] B. Bonin, N. Alamanos, B. Berthier, G. Bruge, H. Faraggi, D. Legrand, J. C. Lugol, W. Mittig, L. Papineau, A. I. Yavin, D. K. Scott, M. Levine, J. Arvieux, L. Farvacque, and M. Buenerd, Nucl. Phys. **A430**, 349 (1984).
[11] P. Doll, D. L. Hendrie, J. Mahoney, A. Menchaca-Rocha, D. K. Scott, M. Symons, K. Van Bibber, Y. P. Viyogi, and H. Weiman, Phys. Rev. Lett. **42**, 366 (1979).
[12] R. L. Neto, P. Roussel-Chomaz, L. Rochais, N. Alamanos, F. Auger, B. Fernandez, J. Gastebois, A. Gillibert, R. Lacey, A. Miczaika, D. Pierroutskou, J. Barrette, S. K. Mark, R. Turcotte, Y. Blumenfeld, N. Frascaria, J. P. Roynette, J. A. Scarpaci, T. Suomijärvi, A. van der Woude, and A. M. Van den Berg, Nucl. Phys. **A560**, 733 (1993).
[13] J. M. Moss, D. R. Brown, D. H. Youngblood, C. M. Rozsa, and J. D. Bronson, Phys. Rev. C **18**, 741 (1978).
[14] D. R. Brown, J. M. Moss, C. M. Rozsa, D. H. Youngblood, and J. D. Bronson, Nucl. Phys. **A313**, 157 (1979).
[15] S. Shlomo, Y.-W. Lui, D. H. Youngblood, T. Udagawa, and T. Tamura, Phys. Rev. C **36**, 1317 (1987).
[16] A. van der Woude, *Electric and Magnetic Giant Resonances* (World Scientific, Singapore, 1991), p. 99.
[17] D. H. Youngblood, J. Bronson, and Y.-W. Lui, ''Progress in Research April 1991–March 1992,'' Cyclotron Institute, Texas A&M University report, 1992, p. 110.
[18] J. S. Winfield, D. M. Pringle, W. N. Catford, D. G. Lewis, and K. W. Allen, Nucl. Instrum. Methods Phys. Res. Sect. A **251**, 297 (1986).
[19] J. L. Blankenship, R. L. Auble, J. R. Beene, F. E. Bertrand,

and D. Shapira, Physics Division Progress Report for the period ending September 30, 1992, Oak Ridge National Laboratory, 1993, p. 89.
[20] D. H. Youngblood, Y.-W. Lui, H. L. Clark, P. Oliver, and G. Simler, Nucl. Instrum. Methods Phys. Res. Sect. A **331**, 539 (1995).
[21] H. L. Clark, D. H. Youngblood, and Y.-W. Lui, Nucl. Phys. **A589**, 416 (1995).
[22] D. M. Pringle, W. N. Catford, J. S. Winfield, D. G. Lewis, N. A. Jelley, K. W. Allen, and J. H. Coupland, Nucl. Instrum. Methods Phys. Res. Sect. A **245**, 230 (1986).
[23] D. H. Youngblood and J. Bronson, Nucl. Instrum. Methods Phys. Res. Sect. A **361**, 37 (1995).
[24] F. Ajzenberg-Selove, Nucl. Phys. **A506**, 1 (1990).
[25] M. Rhoades-Brown, M. H. Macfarlane, and S. C. Pieper, Phys. Rev. C **21**, 2417 (1980); **21**, 2436 (1980); M. H. MacFarlane and S. C. Pieper, Argonne National Laboratory Report No. ANL-76-11, Rev. 1, 1978 (unpublished).
[26] D. H. Youngblood and Y.-W. Lui, Phys. Rev. C **44**, 1878 (1991).
[27] C. M. Rozsa, D. H. Youngblood, J. D. Bronson, Y.-W. Lui, and U. Garg, Phys. Rev. C **21**, 1252 (1980).
[28] J. R. Beene, D. J. Horen, and G. R. Satchler, Phys. Lett. B **344**, 67 (1995).
[29] P. Barreau and J. B. Bellicard, Phys. Rev. Lett. **19**, 1444 (1967).
[30] J. W. Lightbody, Jr., S. Penner, S. P. Fivozinsky, P. L. Hallowell, and H. Crannell, Phys. Rev. C **14**, 952 (1976).
[31] G. R. Satchler, Nucl. Phys. **A472**, 215 (1987).
[32] Received from P. D. Kunz, University of Colorado, Boulder, Colorado.
[33] G. R. Satchler, Part. Nucl. **5**, 105 (1973); Nucl. Phys. **A195**, 1 (1972).
[34] M. N. Harakeh and A. E. L. Dieperink, Phys. Rev. C **23**, 2329 (1981).
[35] A. Bohr and B. R. Mottelson, *Nuclear Structure* (Benjamin, Reading, MA, 1975), Vol. II, p. 600.